

## Do current WIMP direct measurements constrain light relic neutralinos?

A. Bottino, F. Donato, and N. Fornengo

*Dipartimento di Fisica Teorica, Università di Torino, Istituto Nazionale di Fisica Nucleare, via P. Giuria 1, I-10125 Torino, Italy*

S. Scopel

*School of Physics, Korea Institute for Advanced Study, 207-43 Cheongryangri-dong, Dongdaemun-gu, Seoul 130-722, Korea*

(Received 5 September 2005; published 27 October 2005)

New upper bounds on direct detection rates have been presented recently by a number of experimental collaborations working on searches for weakly interacting massive particles (WIMPs). In this paper we analyze how the constraints on relic neutralinos which can be derived from these results are affected by the uncertainties in the distribution function of WIMPs in the halo. Various different categories of velocity distribution functions are considered, and the ensuing implications for supersymmetric configurations derived. We conservatively conclude that current experimental data do not constrain neutralinos of small mass (below 50 GeV).

DOI: [10.1103/PhysRevD.72.083521](https://doi.org/10.1103/PhysRevD.72.083521)

PACS numbers: 95.35.+d, 98.35.Gi, 11.30.Pb, 12.60.Jv

### I. INTRODUCTION

In Refs. [1–4] we have discussed the cosmological properties of light neutralinos (i.e. neutralinos with a mass in the range  $6 \text{ GeV} \lesssim m_\chi \lesssim 50 \text{ GeV}$ ), which originate in supersymmetric schemes where gaugino-mass unification is not assumed. Actually, the most remarkable features occur for neutralinos in the mass range  $6 \text{ GeV} \lesssim m_\chi \lesssim 25 \text{ GeV}$ . Namely, for relic neutralinos with these masses, direct and indirect detection rates are considerably high, and at the level of present experimental sensitivities. Furthermore, the range of the predicted values for the rates is quite narrow—at variance with what happens for neutralinos of higher masses—where the expected rates are spread over decades.

The properties of light neutralinos with respect to weakly interacting massive particle (WIMP) direct measurements were analyzed in Refs. [2,3]. Since then, some new results and/or analyses of previous data from experiments of WIMP direct searches have appeared [5–8]. In the present paper, we examine whether these new data put some constraints on the relic neutralinos of light masses.

Let us recall that the differential event rate  $dR/dE_R$  ( $E_R$  being the nuclear recoil energy) measured in WIMP direct searches is a convolution of the WIMP-nucleus cross section with the WIMP phase-space distribution function, evaluated at the Earth location. By assuming that (i) in this phase-space distribution function, spatial and velocity dependence factorize, and (ii) coherent interactions dominate over incoherent ones in the WIMP-nucleus scattering (which is usually the case for relic neutralinos), one recovers the expression:

$$\frac{dR}{dE_R} = N_T \frac{\rho_0}{m_\chi} \frac{m_N}{2\mu_A^2} A^2 \xi \sigma_{\text{scalar}}^{(\text{nucleon})} F^2(E_R) I(v_{\min}), \quad (1)$$

where

$$I(v_{\min}) = \int_{w \geq v_{\min}} d^3w \frac{f_{\text{ES}}(\vec{w})}{w}. \quad (2)$$

In the previous formulas,  $N_T$  is the number of target nuclei per unit mass,  $m_\chi$  is the WIMP mass,  $m_N$  is the nucleus mass,  $\mu_A$  is the WIMP-nucleon reduced mass,  $A$  the nuclear mass number,  $\sigma_{\text{scalar}}^{(\text{nucleon})}$  is the WIMP-nucleon scalar cross section,  $F(E_R)$  is the nuclear form factor,  $\xi$  is the fraction of the mass density of the WIMP in terms of the total local density for nonbaryonic dark matter  $\rho_0$  (i.e.,  $\xi = \rho_w/\rho_0$ ), and  $\vec{w}$  and  $f_{\text{ES}}(\vec{w})$  denote the WIMP velocity and velocity distribution function (DF) in the Earth frame, respectively, ( $w = |\vec{w}|$ ). It is natural to define the velocity distribution function in the galactic rest frame  $f(\vec{v})$ , where  $\vec{v} = \vec{w} + \vec{v}_\oplus$ ,  $\vec{v}_\oplus$  being the Earth velocity in the galactic rest frame. The Earth frame velocity DF is then obtained by means of the transformation:  $f_{\text{ES}}(\vec{w}) = f(\vec{w} + \vec{v}_\oplus)$ . It is implicitly understood that the velocity DF  $f(\vec{v})$  is truncated at a maximal escape velocity  $v_{\text{esc}}$ , since the gravitational field of the Galaxy cannot bind arbitrarily fast WIMPs. The value we adopt here is  $v_{\text{esc}} = 650 \text{ km sec}^{-1}$  [9], although we will comment on the effect of a lower value, which we will set at  $v_{\text{esc}} = 450 \text{ km sec}^{-1}$  [9]. Finally, the quantity  $v_{\min}$  appearing in Eq. (2) defines the minimal Earth frame WIMP velocity which contributes to a given recoil energy  $E_R$ :

$$v_{\min} = [m_N E_R / (2\mu_A^2)]^{1/2}, \quad (3)$$

where  $\mu_A$  is the WIMP-nucleus reduced mass.

Equations (1) and (2) are the basis for deriving information on the quantity  $\xi \sigma_{\text{scalar}}^{(\text{nucleon})}$  from the measurements on the differential rate  $dR/dE_R$ . However, this procedure implies the use of a specific WIMP distribution function, which determines both the value of the local dark matter density  $\rho_0$  and the shape of the velocity DF  $f(\vec{v})$ .

In the present paper we first discuss how upper bounds on  $\xi \sigma_{\text{scalar}}^{(\text{nucleon})}$ , derived from experimental upper limits on

$dR/dE_R$ , depend on the large uncertainties affecting the WIMP distribution functions. We then discuss what is the relevance of these upper bounds on  $\xi\sigma_{\text{scalar}}^{(\text{nucleon})}$  for light relic neutralinos.

## II. WIMP DISTRIBUTION FUNCTIONS

In our analysis we consider a subset of the large sample of galactic halo models which were studied in detail in Ref. [10]. Following Ref. [10], we classify the DFs into four categories, depending on the symmetry properties of the matter density (or the corresponding gravitational potential) and of the velocity dependence: (A) spherically symmetric matter density  $\rho_{\text{DM}}$  with isotropic velocity dispersion, (B) spherically symmetric matter density with nonisotropic velocity dispersion, (C) axisymmetric models, (D) triaxial models [11,12].

For each category, different specific models are identified. The models considered in the present analysis are listed in Table I. For a thorough definition of the different models and of the values of their intrinsic parameters, and for a detailed description of theoretical technicalities, we refer to Ref. [10]. Here we just remind the reader that for each model we calculate, either analytically (when possible) or numerically, the velocity DF which accompanies a given matter density distribution. For the spherically symmetric and isotropic models of class A, the velocity DF is obtained by solving the Eddington equation [10,17]. For the spherically symmetric and nonisotropic models of class B we assume the anisotropy to be described in terms of the Osipkov-Merrit parameter  $\beta$  [10,17,18] which defines the degree of anisotropy (we fix  $\beta = 0.4$ ): in this

TABLE I. Summary of the galactic halo models considered in our analysis. The label shown in the first column is used throughout the text to indicate each model in a unique way and corresponds to the classification introduced in Ref. [10]. For details on the models and proper definitions, see Ref. [10].

A: Spherical $\rho_{\text{DM}}$ , isotropic velocity dispersion	
A0	Isothermal sphere
A1	Evans's logarithmic [13]
A2	Evans's power law [14]
A5	NFW [15]
B: Spherical $\rho_{\text{DM}}$ , nonisotropic velocity dispersion	
B1	Evans's logarithmic [13]
B2	Evans's power law [14]
B5	NFW [15]
C: Axisymmetric $\rho_{\text{DM}}$	
C2	Evans's logarithmic
C3	Evans's power law
D: Triaxial $\rho_{\text{DM}}$ [16]	
D1	Earth on major axis, radial anisotropy

case, the velocity DF can be obtained by a generalization of the Eddington method [10,17]. Axisymmetric models of class C allow the presence of a definite angular momentum. We choose them as a direct generalization of some of the models of class A: for these models, analytical solutions to the relevant generalized Eddington equation may be found. In this case, we also allow for a maximal corotation or counterrotation of the galactic halo. Finally, class D presents a specific triaxial model.

Each halo model is constrained by a number of observational inputs [10]: (i) properties of the galactic rotational curve, namely, the range of the allowed values for the local rotational velocity,  $170 \text{ km sec}^{-1} \leq v_0 \leq 270 \text{ km sec}^{-1}$  [19,20], and the amount of flatness of the rotational curve at large distances from the galactic center, and (ii) the maximal amount of nonhalo components in the Galaxy,  $M_{\text{vis}}$  (i.e. the disk, the bulge, etc.). These constraints determine first of all the value of the local dark matter density  $\rho_0$ , which is a relevant parameter in the direct detection rate. Depending on whether one allows for a maximal halo (i.e. the contribution of the nonhalo components is minimized) or, the other way around, the contribution of the halo to the rotational curve is minimized, the value of  $\rho_0$  is either increased or reduced, respectively. This is discussed in detail in Ref. [10] and is manifest also in Table II, where values of  $\rho_0$  for each halo model and for the three representative values of  $v_0$  are shown. The difference in the values of  $\rho_0$  depending on the assumption of a minimal or a maximal halo contribution is given in Ref. [10]. For instance, for the isothermal sphere  $\rho_0$  falls in the range  $(0.18, 0.28) \text{ GeV cm}^{-3}$  for  $v_0 = 170 \text{ km sec}^{-1}$ ,  $(0.30, 0.47) \text{ GeV cm}^{-3}$  for  $v_0 = 220 \text{ km sec}^{-1}$ , and  $(0.45, 0.71) \text{ GeV cm}^{-3}$  for  $v_0 = 270 \text{ km sec}^{-1}$ . We therefore expect a significant variability in the extracted upper limits in direct detection experiments also for the simple and generally used isothermal sphere model. We notice that the standard reference choice of  $\rho_0 = 0.30 \text{ GeV cm}^{-3}$  for  $v_0 = 220 \text{ km sec}^{-1}$  refers to the case of a minimal halo.

The choice we make here for the values of  $\rho_0$  associated to each representative value of  $v_0$  is the following: for  $v_0 = 170 \text{ km sec}^{-1}$  (which correspond to its 95% C.L. lower bound) we adopt the case of a minimal halo, in order to determine the set of less constraining upper limits on  $\xi\sigma_{\text{scalar}}^{(\text{nucleon})}$ , as is clear from Eq. (1). For  $v_0 = 270 \text{ km sec}^{-1}$  (which corresponds to its 95% C.L. upper bound) we instead adopt a maximal halo: in this case we will determine the most constraining upper limits on  $\xi\sigma_{\text{scalar}}^{(\text{nucleon})}$ . In the case of the central (and reference) value  $v_0 = 220 \text{ km sec}^{-1}$ , we adopt a minimal halo, which reproduces the standard choice  $\rho_0 = 0.30 \text{ GeV cm}^{-3}$  for the isothermal sphere. These considerations apply to all models of class A and B. For the models of class C and D, for which we can rely only on analytical solutions for the velocity DF, we are forced to use always the case of a

TABLE II. Values of the dark matter local density  $\rho_0$  corresponding to the three different values of the local rotational velocity  $v_0$  and obtained from the constraints on the amount of nonhalo component and on the flatness of the galactic rotational curve, for the different halo models of Table I. For the models of class A and B, the values of  $\rho_0$  are the minimal ones (i.e. corresponding to a minimal halo contribution) for  $v_0 = 170 \text{ km sec}^{-1}$  and  $v_0 = 220 \text{ km sec}^{-1}$ , while for  $v_0 = 270 \text{ km sec}^{-1}$  the values of  $\rho_0$  are the maximal ones (referring to a maximal halo). For models of class C and D, the value of  $\rho_0$  is always the maximal one. The axisymmetric models of class C are not affected by the inclusion of a corotation or counterrotation effect.

	$v_0 = 170 \text{ km sec}^{-1}$	$v_0 = 220 \text{ km sec}^{-1}$	$v_0 = 270 \text{ km sec}^{-1}$
Model	$\rho_0(\text{GeV cm}^{-3})$	$\rho_0(\text{GeV cm}^{-3})$	$\rho_0(\text{GeV cm}^{-3})$
A0	0.18	0.30	0.71
A1 , B1	0.20	0.34	1.07
A2 , B2	0.24	0.41	1.33
A5 , B5	0.20	0.33	1.11
C2	0.67	1.11	1.68
C3	0.66	1.10	1.66
D1	0.50	0.84	1.27

maximal halo: in fact, analytical solutions of class C and D are actually obtained only for a maximal halo contribution [10].

Let us turn now to the direct effect of the velocity DF on the detection rate, which is studied here in terms of the relevant function  $I(v_{\min})$  of Eq. (2). Figure 1 shows  $I(v_{\min})$  for the isothermal halo and for the three values

of  $v_0$  listed in Table II. We see that for low values of  $v_{\min}$  the larger contribution to the detection rate occurs when  $v_0$  is smaller, since for smaller rotational velocities the velocity dispersion of the isothermal Maxwellian distribution is also smaller, and in turn this enhances the average inverse velocity, which is related to the definition of  $I(v_{\min})$ :  $\langle 1/w \rangle = I(0)$ . This can be analytically understood by remembering that for a pure isothermal sphere and a maximal halo the velocity distribution function is just an isotropic Maxwellian with velocity dispersion given by  $v_0$ :

$$f_A(v) = [\pi v_0^2]^{-3/2} \exp(-v^2/v_0^2); \quad (4)$$

in this case the function  $I(v_{\min})$  reads (in the limit  $v_{\text{esc}} \rightarrow \infty$ ) [21]:

$$I(v_{\min}) = \frac{1}{2\eta v_0} [\text{erf}(x_{\min} + \eta) - \text{erf}(x_{\min} - \eta)], \quad (5)$$

where  $x_{\min} = v_{\min}/v_0$  and  $\eta = v_{\oplus}/v_0$ . From Eq. (5) we see that for small values of  $v_{\min}$  the larger  $I(v_{\min})$  occurs for smaller  $v_0$  because of the inverse law dependence.

On the contrary, for large values of  $v_{\min}$ , the almost exponential tail in  $I(v_{\min})$  is more severe when  $v_0$  is small, and therefore the behavior of  $I(v_{\min})$  with respect to  $v_0$  is the opposite. This again is understood from the simple expression of Eq. (5). The regime we are considering ( $v_{\min} \gtrsim v_{\oplus}$ ) asymptotically can be studied as the limit  $\eta \rightarrow 0$  in Eq. (5), which gives:

$$I(v_{\min}) = 2[\pi v_0^2]^{-1/2} \exp(-v_{\min}^2/v_0^2). \quad (6)$$

The tail, due to the presence of a nonvanishing  $\eta$  in Eq. (5), is less severe than the one in Eq. (6) but nevertheless it follows the same behavior.

Also the value of the escape velocity is relevant in the large  $v_{\min}$  tail of the function  $I(v_{\min})$ . The results presented so far in Fig. 1 are obtained for a value of the escape velocity (in the galactic frame)  $v_{\text{esc}} = 650 \text{ km sec}^{-1}$ .

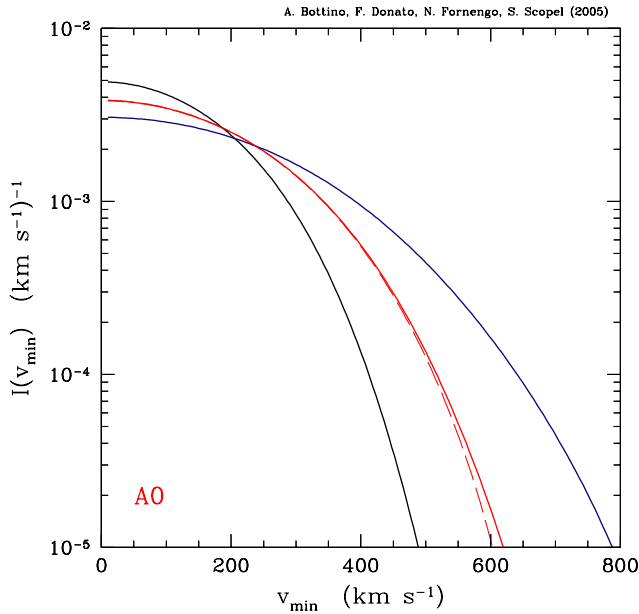


FIG. 1 (color online). Function  $I(v_{\min})$  for an isothermal sphere (model A0 of Table I) and  $v_{\text{esc}} = 650 \text{ km sec}^{-1}$ . The solid curves (from top to bottom, as seen on the extreme left of the plot) refer to the three values of  $v_0$  (and ensuing  $\rho_0$ ) given in Table II:  $v_0 = 170 \text{ km sec}^{-1}$  (top),  $v_0 = 220 \text{ km sec}^{-1}$  (middle),  $v_0 = 270 \text{ km sec}^{-1}$  (bottom). The dashed line shows the modification of the median isothermal case when  $v_{\text{esc}} = 450 \text{ km sec}^{-1}$ .

However, values as low as  $v_{\text{esc}} = 450 \text{ km sec}^{-1}$  also have been considered [9]. A lower escape velocity implies a cut in the high  $v_{\text{min}}$  tail of  $I(v_{\text{min}})$  [21]. This effect is shown in Fig. 1 for the central case  $v_0 = 220 \text{ km sec}^{-1}$ .

The discussion on the behavior of  $I(v_{\text{min}})$  has direct impact on the direct detection rate, since  $v_{\text{min}}$  is directly related to the recoil energy. Equation (3) implies that very light WIMPs can produce recoil energies in the tens of keV range only if they possess large velocities. In this case, the detection rate for such light WIMPs will be mostly determined by the almost exponential tail in the function  $I(v_{\text{min}})$  discussed above. On the contrary, heavy WIMPs can produce recoil in the same tens of keV range by possessing much lower velocities: they will be therefore more sensitive also to the low  $v_{\text{min}}$  part of the function  $I(v_{\text{min}})$ . The quantitative connection between  $v_{\text{min}}$  and  $E_R$  for a Ge nucleus and different WIMP masses is given in Fig. 2.

Finally, Fig. 3 shows the function  $I(v_{\text{min}})$  for all the other halo models listed in Table I. As for the symmetric and isotropic models, we see that in the case of a power-law behavior of the gravitational potential (model A2) or for the Navarro-Frenk-White (NFW) density profile (model A5) the large  $v_{\text{min}}$  tail is less suppressed, mainly for low  $v_0$ : this comes along with a larger predicted detection rate and it will translate into a more constraining upper limit for WIMPs lighter than a few tens of GeV. In the case of anisotropic models we notice that the most direct anisotropic generalization of the isothermal sphere, which is a cored spherical distribution with anisotropic velocity dis-

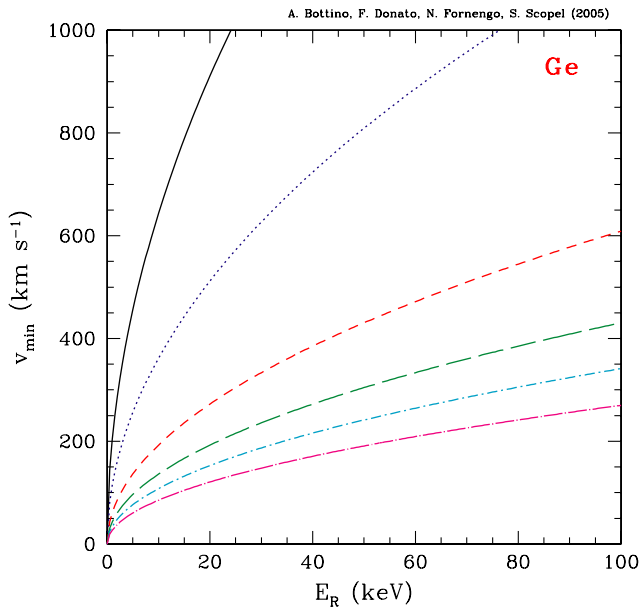


FIG. 2 (color online). Values of  $v_{\text{min}}$  as a function of the nuclear recoil energy  $E_R$  for a Ge detector. The different curves refer to WIMP masses of 10, 20, 50, 100, 200 GeV and 1 TeV, from top to bottom.

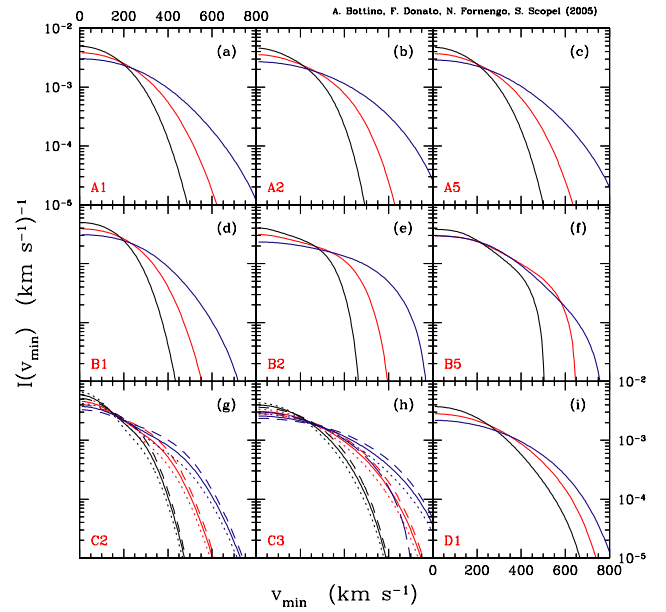


FIG. 3 (color online). Function  $I(v_{\text{min}})$  for all the galactic models of Table I, other than the isothermal sphere, for  $v_{\text{esc}} = 650 \text{ km sec}^{-1}$ . The label which identifies the model is written in the bottom left corner of each panel. Notations are as in Fig. 1. In panels (g) and (h), which correspond to axisymmetric models, the dotted and dashed lines refer to maximal galactic corotation and counterrotation, respectively. In panel (h), the long dashed line shows the modification of the  $v_0 = 270 \text{ km sec}^{-1}$  case when  $v_{\text{esc}} = 450 \text{ km sec}^{-1}$ .

persion (model B1), is the one which is more suppressed at large  $v_{\text{min}}$ : this has the effect of reducing the sensitivity of the detector to light WIMPs. On the contrary, the axisymmetric model with a power-law gravitational potential C3 is the one with the highest tail in the function  $I(v_{\text{min}})$  and therefore more sensitive in constraining light WIMPs. We also notice that for this type of models, which possess an enhanced  $v_{\text{min}}$  tail, the effect of a lower escape velocity is more dramatic: Fig. 3(h) shows the sizeable reduction of  $I(v_{\text{min}})$  at large  $v_{\text{min}}$  for an escape velocity  $v_{\text{esc}} = 450 \text{ km sec}^{-1}$  in the case of model C3 and  $v_0 = 270 \text{ km sec}^{-1}$ .

The local matter density values  $\rho_0$  of Table II and the results of Figs. 1 and 3 are the key elements which will be used in the next section to determine upper limits on the WIMP-nucleon scattering cross sections.

### III. RESULTS AND CONCLUSIONS

In Refs. [5–8] upper limits on  $\xi \sigma_{\text{scalar}}^{\text{(nucleon)}}$  are obtained by using a standard isothermal distribution function with density parameter  $\rho_0 = 0.3 \text{ GeV cm}^{-3}$  and  $v_0 = 220 \text{ km sec}^{-1}$ . Here, we analyze this class of experimental data employing the sample of distribution functions discussed in the previous section. Our analysis and discussion is performed in terms of the experimental data of Ref. [8] (CDMS), since these turn out to be the most constraining

ones. For very light WIMPs, with masses below 10 GeV, also the results of Ref. [7] (ZEPLIN) may play a role, and we will add them in our final discussion.

In order to obtain the exclusion plot from the CDMS data, we extract the neutralino-nucleon cross section that yields a number of events compatible with zero between 10 and 64 keV with an effective exposure  $(MT)_{\text{eff}} = 19.4 \text{ kg} \times \text{day}$ , which corresponds to the effective exposure for  $m_\chi = 60 \text{ GeV}$  quoted in Ref. [8]. By considering a Poissonian fluctuation of the expected rate, we assume the upper bound of 2.3 events at 90% C.L. In the calculation of the expected rate, we use a Helm nuclear form factor and a bolometric quenching factor equal to 1, as quoted by the experimental collaboration [8]. Our procedure for extracting the exclusion plot is less refined than the one adopted in Ref. [8], since it neglects the dependence of  $(MT)_{\text{eff}}$  on the WIMP mass and does not take into account the part of the CDMS spectrum between 64 and 100 keV (which can be included following for instance the statistical procedure of Ref. [22]). Nevertheless our procedure allows us to reproduce to a good degree of precision the CDMS limit for the standard isothermal distribution, as shown by the central curve in Fig. 4, when this is compared with the upper bound displayed in Fig. 39 of Ref. [8]. Therefore, in our analysis we adopt our simpler procedure; we have checked that adding a proper treatment of the efficiency and adopting the statistical procedure of Ref. [22] yields quite similar results.

The upper limits for the isothermal sphere (model A0) are shown in Fig. 4, for the three representative values of  $v_0$  and the corresponding choices for the local dark matter density  $\rho_0$ , as quoted in Table II. As already mentioned, the central curve corresponds to the reference case of  $v_0 = 220 \text{ km sec}^{-1}$  with  $\rho_0 = 0.3 \text{ GeV cm}^{-3}$ . The upper and lower curves are instead obtained for  $v_0 = 170 \text{ km sec}^{-1}$  with  $\rho_0 = 0.18 \text{ GeV cm}^{-3}$  and  $v_0 = 270 \text{ km sec}^{-1}$  with  $\rho_0 = 0.71 \text{ GeV cm}^{-3}$ , respectively. An important effect is obviously due to the different values of  $\rho_0$  which are associated to the different values of  $v_0$ , as discussed in the previous section and in Ref. [10]. However, the difference in the function  $I(v_{\text{min}})$  is quite relevant in the determination of the upper limits, especially at low WIMP masses. In order to appreciate the difference in the exclusion plots, we show in Fig. 5 the ratios of the upper limits obtained with  $v_0 = 170 \text{ km sec}^{-1}$  (upper curve) and  $v_0 = 270 \text{ km sec}^{-1}$  (lower curve) with respect to the central  $v_0 = 220 \text{ km sec}^{-1}$  case. The dashed horizontal lines show the ratios of the corresponding values of  $\rho_0$ . We notice that at low WIMP masses the difference in the exclusion plots is very large, much larger than the naïve ratio of the corresponding  $\rho_0$ 's. This is a consequence of the sizable difference in  $I(v_{\text{min}})$  for large  $v_{\text{min}}$ , which is the regime relevant for light WIMPs, as discussed before.

On the contrary, at large WIMP masses, the difference in the exclusion plots is much closer to what one would

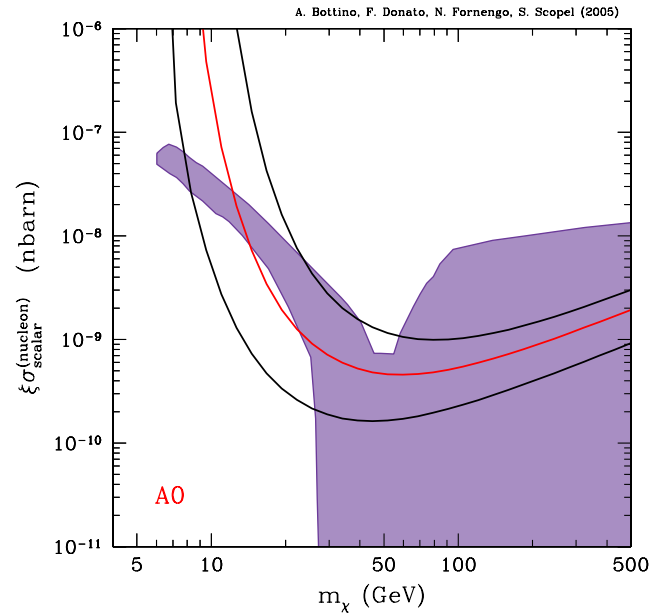


FIG. 4 (color online). The solid lines show the upper limit on the quantity  $\xi\sigma_{\text{scalar}}^{(\text{nucleon})}$  as a function of the WIMP mass  $m_\chi$  for the CDMS detector and for an isothermal sphere (model A0 of Table I). The curves refer to the three values of  $v_0$  (and corresponding  $\rho_0$ ) given in Table II:  $v_0 = 170 \text{ km sec}^{-1}$  (top),  $v_0 = 220 \text{ km sec}^{-1}$  (middle),  $v_0 = 270 \text{ km sec}^{-1}$  (bottom). The shaded region shows the values of  $\xi\sigma_{\text{scalar}}^{(\text{nucleon})}$  for neutralino dark matter, obtained in a scan of the minimal supersymmetric model defined in Refs. [1–4]. The funnel for low neutralino masses (below 50 GeV) corresponds to supersymmetric models without gaugino-mass unification.

expect on the basis of the difference in the  $\rho_0$  values. This is clear from our previous analysis, since for large WIMP masses the relevant range of  $v_{\text{min}}$  is in the 100–300  $\text{km sec}^{-1}$  range, which is where the difference in  $I(v_{\text{min}})$  is small. We can notice also that, for large WIMP masses, it is even possible to revert the value of the ratio of the exclusion plots naïvely obtained by the ratio of the different  $\rho_0$ 's: this is a consequence of the behavior of  $I(v_{\text{min}})$  at small  $v_{\text{min}}$  discussed in the previous section.

Figure 4 represents the maximal variability which occurs for the isothermal sphere: this quantifies the astrophysical uncertainty connected to this halo model. Confronting the upper limits with the results obtained for light neutralinos in supersymmetric models without gaugino-mass universality [1–4], we can see that while all the configurations in the mass range  $15(8) \text{ GeV} \leq m_\chi \leq 25 \text{ GeV}$  are excluded for the central (upper) values of  $v_0$ , only a small fraction is eliminated when  $v_0$  assumes its lower bound value. Therefore, the conservative attitude which has to be taken when setting limits makes us to conclude that for the isothermal sphere, direct detection only mildly constrains the light neutralino sector of supersymmetric models without gaugino-mass universality [1–

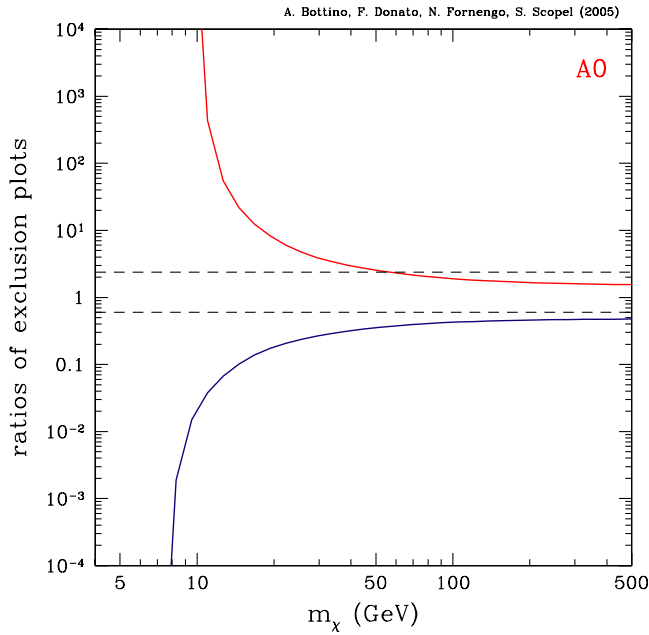


FIG. 5 (color online). Ratios of the upper limits of Fig. 4, obtained for an isothermal sphere (model A0). The upper curve is the ratio between the upper (obtained for  $v_0 = 170 \text{ km sec}^{-1}$ ) and the central ( $v_0 = 220 \text{ km sec}^{-1}$ ) curves in Fig. 4. The lower curve is the ratio between the lower ( $v_0 = 270 \text{ km sec}^{-1}$ ) and central curves in Fig. 4. The dashed horizontal lines show the ratios of the corresponding values of  $\rho_0$ .

4], in the 20–40 GeV mass range. Clearly the variation on the upper limits due to the difference in the halo properties has consequences also on the exploration of the supersymmetric parameter space for heavier neutralinos, as is shown in Fig. 4. This is relevant also to gaugino-mass universal models, for which the lower bound on the neutralino mass exceeds 50 GeV [23].

The results for the other galactic halo models is shown in Fig. 6. The differences in the upper limits can be understood on the basis of the discussion on the isothermal sphere and on the properties of  $I(v_{\min})$  for the different models presented in the previous section. We notice that some models, like C3, D1, and B5 are more constraining, while in the case of models like A1 and B1 the limits imposed by direct detection are relatively less severe.

Finally, we report in Fig. 7 the summary of our analysis: together with the standard central isothermal sphere, we show the more (C3) and less (B1) constraining models we obtain. From the analysis of this figure, we conservatively conclude that from direct detection experiments there is currently no constraint on the light neutralino sector of supersymmetric models without gaugino universality [1–4]. Should the local value of the rotational velocity be on its high range (close to  $v_0 = 270 \text{ km sec}^{-1}$ ) direct detection could be able to set stringent limits on these supersymmetric configurations: all the mass range above 7–8 GeV (depending on the actual halo model) and below 25 GeV

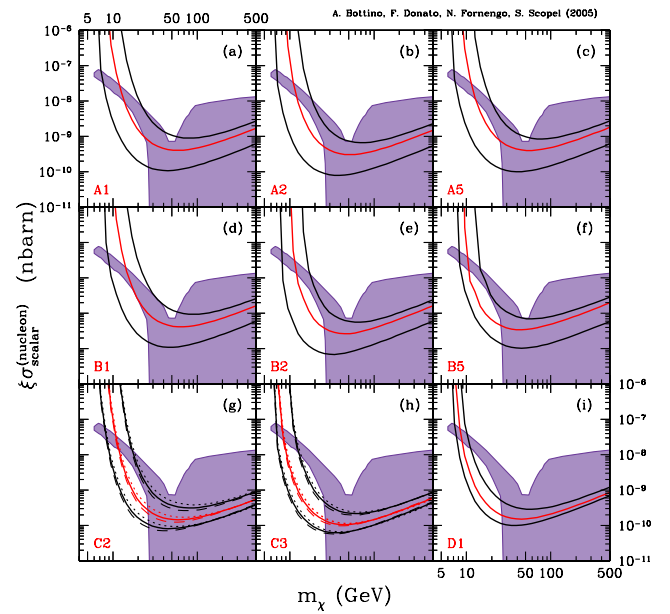


FIG. 6 (color online). The solid lines show the upper limit on the quantity  $\xi \sigma_{\text{scalar}}^{(\text{nucleon})}$  as a function of the WIMP mass  $m_\chi$  for the CDMS detector and for the different galactic models of Table I, other than the isothermal sphere. The label which identifies the model is shown in the bottom left corner of each panel. Notations are as in Fig. 4. In panels (g) and (h), which correspond to axisymmetric models, the dotted and dashed lines refer to maximal galactic corotation and counterrotation, respectively.

would be excluded. Notice that, would this be the case, also the local density  $\rho_0$  would be large (above  $0.7 \text{ GeV cm}^{-3}$ , as discussed in Ref. [10] and shown in Table II); in this case the neutralino configurations below 7–8 GeV, which are not constrained by direct detection, would be completely excluded by antiproton searches [4]. However, due to astrophysical uncertainties which affect the different detection rates, currently it is not yet possible to set absolute limits, neither from indirect detection techniques [3,4] or, as shown in the present analysis, by direct detection.

Figure 7 also shows the effect of a lower escape velocity. As discussed in the previous section, this implies a cut in the high  $v_{\min}$  tail of  $I(v_{\min})$ : this turns into a weaker sensitivity of direct detection to low-mass neutralinos. The effect is especially manifest for the most stringent models, like model C3 with  $v_0 = 270 \text{ km sec}^{-1}$ . For  $v_{\text{esc}} = 450 \text{ km sec}^{-1}$ , all neutralino models below 9 GeV are not constrained even for C3 model. For the A0 model with  $v_0 = 220 \text{ km sec}^{-1}$ , there is also a sizeable difference for light WIMPs, although this is not relevant for the neutralino configurations. Finally, in the case of model B1 with  $v_0 = 170 \text{ km sec}^{-1}$ , the lower escape velocity does not produce differences, since in the high-velocity tail  $I(v_{\min})$  was already depressed even for  $v_{\text{esc}} = 650 \text{ km sec}^{-1}$ , as can be seen in Fig. 3.

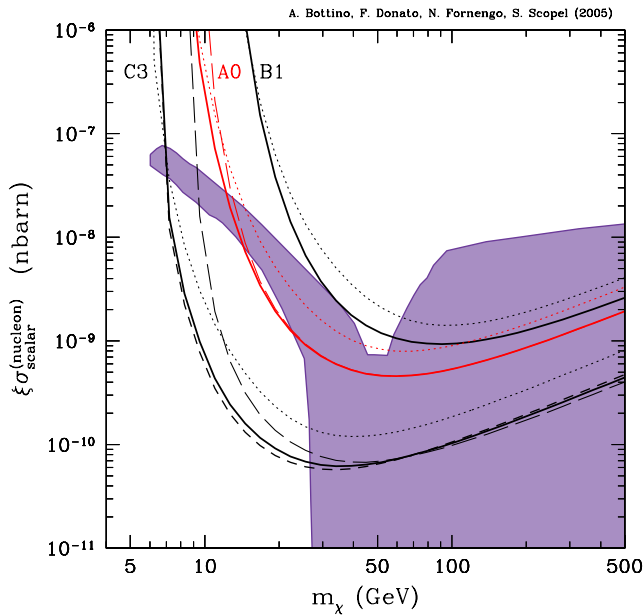


FIG. 7 (color online). The solid lines show the summary of our analysis on the upper limit on the quantity  $\xi\sigma_{\text{scalar}}^{(\text{nucleon})}$  as a function of the WIMP mass  $m_\chi$  for the CDMS detector and for  $v_{\text{esc}} = 650 \text{ km sec}^{-1}$ . The median line refers to the standard isothermal sphere with  $v_0 = 220 \text{ km sec}^{-1}$  and  $\rho_0 = 0.3 \text{ GeV cm}^{-3}$  (model A0). The upper and lower curves show the two extremes obtained in the analysis and refer to model B1 with  $v_0 = 170 \text{ km sec}^{-1}$  (upper solid line) and model C3 with  $v_0 = 270 \text{ km sec}^{-1}$  (lower solid line). The dashed line refers to model C3 with maximal counterrotation of the galactic halo. The dotted lines show the ZEPLIN I limits obtained for the same galactic models. The long dashed lines show the upper limits for CDMS in the case of a lower escape velocity  $v_{\text{esc}} = 450 \text{ km sec}^{-1}$ : the upper line refers to model A0, the lower one to model C3. For model B1, the limit coincides with the corresponding solid line. The shaded region shows the values of  $\xi\sigma_{\text{scalar}}^{(\text{nucleon})}$  for neutralino dark matter, obtained in a scan of the minimal supersymmetric model defined in Refs. [1–4]. The funnel for low neutralino masses (below 50 GeV) corresponds to supersymmetric models without gaugino-mass unification.

For completeness, Fig. 7 also shows the upper limits we obtain for the ZEPLIN detector [7], for the isothermal

sphere and for the two extreme cases. The limits we obtain for the isothermal sphere are slightly higher at low WIMP masses than the ones quoted by the experimental collaboration [7]. We trace this effect to some differences in the analysis of the data (we do not make use of the “light response matrix” discussed in Ref. [7] since we do not have it at our disposal). Figure 7 shows that for very low WIMP masses ZEPLIN could be slightly more sensitive than CDMS. Nevertheless, even lowering by a factor of 2 the upper limits we obtain for ZEPLIN, our conclusions on the limits imposed to light neutralinos remain unchanged.

Finally, we wish to remind that an annual modulation effect in direct detection has been observed by the DAMA Collaboration over seven years [24]. This result, when interpreted in terms of scalar WIMP-nucleus interactions, leads to an allowed region in the plane  $\xi\sigma_{\text{scalar}}^{(\text{nucleon})}$  vs  $m_\chi$ , which extends also to light WIMP masses. The DAMA Collaboration analysis of Ref. [24] takes into account the same variability in galactic halo models of Ref. [10] as the one used here. It is not possible to make direct comparison among the DAMA allowed region and the upper limits we obtain here for CDMS and ZEPLIN, since the DAMA region is the convolution obtained after varying all the galactic halo models, while the results presented here refer to single halo models. A proper comparison between different experimental results can be made *only* at a fixed galactic halo model. Notice that a convolution of our results would be just the upper curve (model B1) of Fig. 7.

As for the comparison between the light neutralinos of nonuniversal gaugino models and the DAMA allowed region, we remind the reader that these light neutralinos are totally compatible with the allowed DAMA region, as we showed in Ref. [2]: they could in fact explain the annual modulation effect.

## ACKNOWLEDGMENTS

We gratefully acknowledge support provided by Research Grants of the Italian Ministero dell’Istruzione, dell’Università e della Ricerca (MIUR), of the Università di Torino, and of the Istituto Nazionale di Fisica Nucleare (INFN) within the *Astroparticle Physics Project*.

- 
- [1] A. Bottino, N. Fornengo, and S. Scopel, Phys. Rev. D **67**, 063519 (2003).
  - [2] A. Bottino, F. Donato, N. Fornengo, and S. Scopel, Phys. Rev. D **68**, 043506 (2003); Phys. Rev. D **69**, 037302 (2004).
  - [3] A. Bottino, F. Donato, N. Fornengo, and S. Scopel, Phys. Rev. D **70**, 015005 (2004).
  - [4] A. Bottino, F. Donato, N. Fornengo, and P. Salati, hep-ph/0507086.
  - [5] G. Angloher *et al.* (CRESST Collaboration), Astropart. Phys. **23**, 325 (2005).
  - [6] V. Sanglard *et al.* (EDELWEISS Collaboration), Phys. Rev. D **71**, 122002 (2005).
  - [7] G.J. Alner *et al.* (UK Dark Matter Collaboration), Astropart. Phys. **23**, 444 (2005).
  - [8] D.S. Akerib *et al.* (CDMS Collaboration) astro-ph/0507190.
  - [9] P.J.T. Leonard and S. Tremaine, Astrophys. J. **353**, 486

- (1990).
- [10] P. Belli, R. Cerulli, N. Fornengo, and S. Scopel, *Phys. Rev. D* **66**, 043503 (2002).
- [11] The class of models discussed in Ref. [10] represents a quite exhaustive summary of dark matter distribution functions as possible departures from the isothermal sphere model. Notice, however, that it does not include the possibility of nonthermal components in the  $f(\vec{v})$ , which could in principle modify the high-velocity tail of the velocity DF (see, for instance: A. Helmi, S. D. M. White, V. Springel, *Phys. Rev. D* **66**, 063502 (2002)).
- [12] For other analyses, see for instance: A. M. Green, *Phys. Rev. D* **68**, 023004 (2003); **69**, 109902(E) (2004); A. M. Green, *Phys. Rev. D* **66**, 083003 (2002); A. M. Green, *Phys. Rev. D* **63**, 043005 (2001); M. Kamionkowski and A. Kinkhabwala, *Phys. Rev. D* **57**, 3256 (1998); J. D. Vergados, *Phys. Rev. Lett.* **83**, 3597 (1999); J. D. Vergados and D. Owen, *Astrophys. J.* **589**, 17 (2003); P. Ullio and M. Kamionkowski, *J. High Energy Phys.* 03 (2001) 049; J. Edsjo, M. Schelke, and P. Ullio, *J. Cosmol. Astropart. Phys.* 09 (2004) 004; G. Gelmini and P. Gondolo, *Phys. Rev. D* **63**, 036006 (2001).
- [13] N. W. Evans, *Mon. Not. R. Astron. Soc.* **260**, 191 (1993).
- [14] N. W. Evans, *Mon. Not. R. Astron. Soc.* **267**, 333 (1994).
- [15] J. F. Navarro, C. S. Frenk, and S. D. M. White, *Astrophys. J.* **462**, 563 (1996).
- [16] N. W. Evans, C. M. Carollo, and P. T. de Zeeuw, *Mon. Not. R. Astron. Soc.* **318**, 1131 (2000).
- [17] J. Binney and S. Tremaine, *Galactic Dynamics*, (Princeton University Press, Princeton, NJ, 1987).
- [18] L. P. Osipkov, *Pris'ma Astron.* **55**, 77 (1979); D. Merrit, *Astrophys. J.* **90**, 1027 (1985).
- [19] C. S. Kochanek, *Astrophys. J.* **457**, 228 (1996).
- [20] M. Feast and P. Whitelock, *Mon. Not. R. Astron. Soc.* **291**, 683 (1997).
- [21] F. Donato, N. Fornengo, and S. Scopel, *Astropart. Phys.* **9**, 247 (1998).
- [22] S. Yellin, *Phys. Rev. D* **66**, 032005 (2002).
- [23] See for instance: V. Berezhinsky, A. Bottino, J. R. Ellis, N. Fornengo, G. Mignola, and S. Scopel, *Astropart. Phys.* **5**, 1 (1996); A. Bottino, F. Donato, N. Fornengo, and S. Scopel, *Phys. Rev. D* **63**, 125003 (2001); J. R. Ellis, K. A. Olive, Y. Santoso, and V. C. Spanos, *Phys. Rev. D* **71**, 095007 (2005); E. Accomando, R. Arnowitt, B. Dutta, and Y. Santoso, *Nucl. Phys.* **B585**, 124 (2000); U. Chattopadhyay, A. Corsetti, and P. Nath, *Phys. Rev. D* **68**, 035005 (2003); J. L. Feng, K. T. Matchev, and F. Wilczek, *Phys. Lett. B* **482**, 388 (2000); L. Bergstrom and P. Gondolo, *Astropart. Phys.* **5**, 263 (1996); Y. G. Kim, T. Nihei, L. Roszkowski, and R. Ruiz de Austri, *J. High Energy Phys.* 12 (2002) 034; V. A. Bednyakov and H. V. Klapdor-Kleingrothaus, *Phys. Rev. D* **62**, 043524 (2000).
- [24] R. Bernabei *et al.* (DAMA Collaboration), *Riv. Nuovo Cimento* **26N1**, 1 (2003).